

# Exploiting spatial dimensions to enable parallelized continuous directed evolution

Ting Wei<sup>1,\*</sup>, Wangsheng Lai<sup>1,†</sup>, Qian Chen<sup>1,2,†</sup>, Yi Zhang<sup>1,†</sup>, Chenjian Sun<sup>1,2</sup>, Xionglei He<sup>3</sup>, Guoping Zhao<sup>1,4</sup>, Xiongfei Fu<sup>1,2,\*\*</sup> & Chenli Liu<sup>1,2,\*\*\*</sup>

## Abstract

Current strategies to improve the throughput of continuous directed evolution technologies often involve complex mechanical fluid-controlling system or robotic platforms, which limits their popularization and application in general laboratories. Inspired by our previous study on bacterial range expansion, in this study, we report a system termed SPACE for rapid and extensively parallelizable evolution of biomolecules by introducing spatial dimensions into the landmark phage-assisted continuous evolution system. Specifically, M13 phages and chemotactic *Escherichia coli* cells were closely inoculated onto a semisolid agar. The phages came into contact with the expanding front of the bacterial range, and then comigrated with the bacteria. This system leverages competition over space, wherein evolutionary progress is closely associated with the production of spatial patterns, allowing the emergence of improved or new protein functions. In a prototypical problem, SPACE remarkably simplified the process and evolved the promoter recognition of T7 RNA polymerase (RNAP) to a library of 96 random sequences in parallel. These results establish SPACE as a simple, easy to implement, and massively parallelizable platform for continuous directed evolution in general laboratories.

**Keywords** bacteriophage; directed evolution; range expansion; spatial competition; virus spreading

**Subject Categories** Methods & Resources; Microbiology, Virology & Host Pathogen Interaction

**DOI** 10.15252/msb.202210934 | Received 24 January 2022 | Revised 2 September 2022 | Accepted 5 September 2022

**Mol Syst Biol. (2022) 18: e10934**

## Introduction

Directed evolution mimics natural evolution and typically proceeds with iterative rounds of genotype diversification and selection for

desired phenotype activity (Bloom & Arnold, 2009). The steps required in the library construction and selection/screening cycles of conventional directed evolution methods are generally labor-intensive and time-consuming. In order to improve the efficiency and reduce manual labor, researchers are exploring to bring in sophisticated mechanical instruments such as microfluidic/millifluidic systems (Agresti *et al.*, 2010; Fallah-Araghi *et al.*, 2012; Wong *et al.*, 2018) and automated robotic platforms (Pham *et al.*, 2017; Piatkevich *et al.*, 2018; Chory *et al.*, 2021). Continuous directed evolution methods, on the other hand, employ delicate biological designs to enable autonomous cycles of mutant library construction and selection by coupling gene functions of interest to the fitness of replicating organisms (Esvelt *et al.*, 2011; Crook *et al.*, 2016; Ravikumar *et al.*, 2018; English *et al.*, 2019), leading to rapid optimization of biomolecules with little human intervention required. One representative of these methods, phage-assisted continuous evolution (PACE) has been applied to evolve a wide range of protein functions such as the specificity of RNA polymerase, TALEN, and Cas9, target specificity and drug resistance of proteases, activity and target compatibility of base editors, and improved soluble expression of proteins (Esvelt *et al.*, 2011; Carlson *et al.*, 2014; Dickinson *et al.*, 2014; Hubbard *et al.*, 2015; Badran *et al.*, 2016; Bryson *et al.*, 2017; Packer *et al.*, 2017; Hu *et al.*, 2018; Wang *et al.*, 2018; Thuronyi *et al.*, 2019; Richter *et al.*, 2020; Blum *et al.*, 2021). It links the desired property of biomolecules to phage propagation to enable rapid rounds of evolution, and utilizes a chemostat-like apparatus (upper panel, Fig 1A) to constantly supply both uninfected host bacterial cells and a continuously diluted environment for selection. Although the PACE system has been brilliantly designed, the complexity of continuous culturing apparatus and requisite process control make it challenging to perform continuous directed evolution in a highly parallelized form (d'Oelsnitz & Ellington, 2018) unless it is facilitated with robotic platforms (DeBenedictis *et al.*, 2022). This limits its use for important application tasks such as evolution toward multiple targets and in different conditions, or high experimental replication to map evolutionary trajectories (Harms & Thornton, 2013) in general

1 CAS Key Laboratory for Quantitative Engineering Biology, Shenzhen Institute of Synthetic Biology, Shenzhen Institutes of Advanced Technology, Chinese Academy of Sciences, Shenzhen, China

2 University of Chinese Academy of Sciences, Beijing, China

3 State Key Laboratory of Biocontrol, School of Life Sciences, Sun Yat-Sen University, Guangzhou, China

4 CAS Key Laboratory for Synthetic Biology, Institute of Plant Physiology and Ecology, Shanghai Institutes for Biological Sciences, Chinese Academy of Sciences, Shanghai, China

\*Corresponding author. Tel: +86 755 86585245; E-mail: ting.wei@siat.ac.cn

\*\*Corresponding author. Tel: +86 755 86585243; E-mail: xiongfei.fu@siat.ac.cn

\*\*\*Corresponding author. Tel: +86 755 86585245; E-mail: cl.liu@siat.ac.cn

†These authors contributed equally to this work

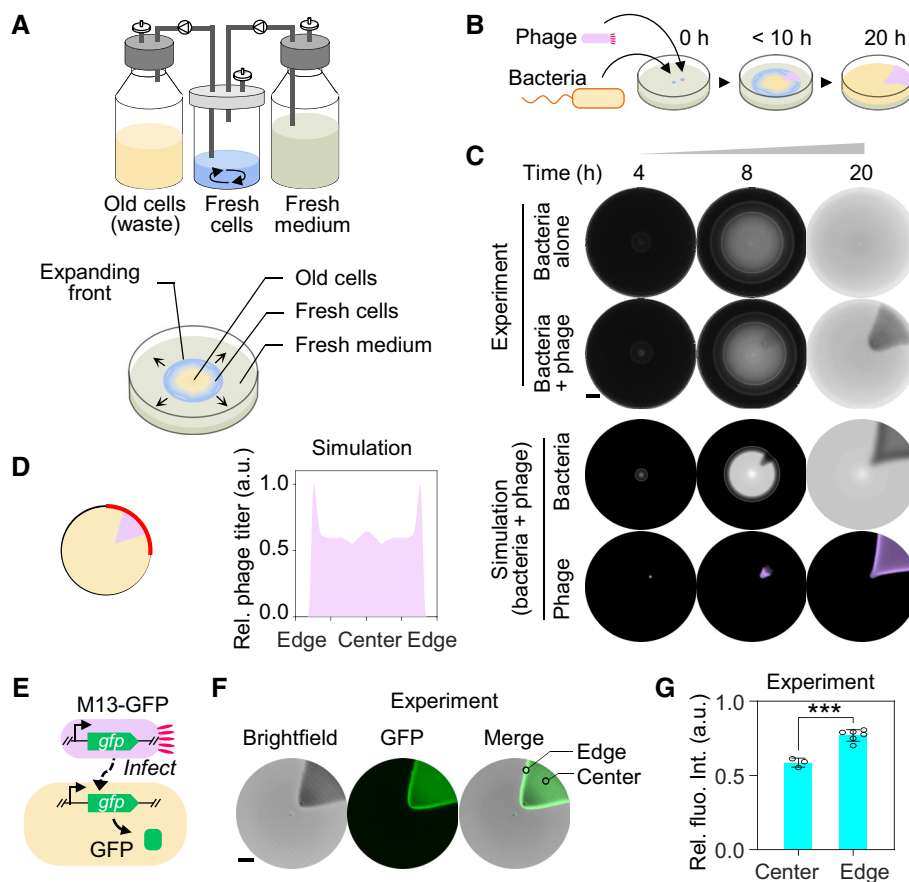


**Figure 1. Formation of the fan-shaped pattern by phage infection during bacterial range expansion.**

- A Illustration of the analogy between bacterial range expansion in a semisolid agar plate and a chemostat-like continuous culturing device.
- B Phage propagation during bacterial range expansion leads to the formation of a visible fan-shaped region of lower cell density.
- C Time-lapse photographs of typical patterns obtained for bacteria alone and bacteria with phage, with corresponding model simulations. Scale bar represents 1 cm.
- D The plot of the simulated phage-titer profile along bacterial expanding front at the time point of 24 h. The position of expanding front is shown by the red arc line in the schematic.
- E Design of a reporter phage M13-GFP for fluorescence imaging of phage-infected region.
- F Visualization of infected region. *Escherichia coli* FM15 was inoculated at the center of a semisolid agar plate and the reporter phage M13-GFP was inoculated 1-cm away from the center. Fluorescence images (Materials and Methods) were captured after overnight incubation using FITC channel and an exposure time of 200 ms. Scale bar represents 1 cm.
- G Relative fluorescence intensity at the center and edge positions of the infection zone as shown in (F). The relative intensity was obtained by dividing the detected values with the maximum value of green fluorescence intensity on the plate. Data represent mean values  $\pm$  s.d. for three values of the center and six values of the edge from three biological replicates. Two-tailed *t*-test was used to compare two groups. \*\*\* $P = 0.0005$ .

Source data are available online for this figure.

laboratories not equipped with sophisticated microfluidic or robotic instruments.

The once-humble agar plate is increasingly seen as a useful platform that can address questions not amenable to study by standard “well-mixed” liquid culture (Baym *et al.*, 2016; Bosshard *et al.*, 2017; Fraebel *et al.*, 2017; Ni *et al.*, 2017; Shih *et al.*, 2018; Liu *et al.*, 2019). For instance, it has recently been utilized to study the evolution of antibiotic resistance (Baym *et al.*, 2016) and the colonization strategies of bacterial range expansion (Liu *et al.*, 2019). In such studies, bacterial cells are typically inoculated at the center or edge of the semisolid agar plate. The subsequent range expansion of bacteria is led by a propagating front of growing cells (blue circle in lower panel of Fig 1A) moving outward toward the uncolonized territory,

while cells with lower motility are left behind to grow until the nutrients are exhausted (Cremer *et al.*, 2019). The steadily advancing front and associated growing wake thus provide a “moving chemostat” that harbors exponentially growing fresh cells (Koster *et al.*, 2012; Cremer *et al.*, 2019), with spontaneous separation from old cells whose growth and motility slow dramatically as nutrients are depleted (lower panel, Fig 1A).

In this study, we sought to develop a new method that combines the advantages of spatial range expansion and PACE. Compared with conventional methods where evolution plays out only on the temporal dimension, bringing in spatial dimensions enables visualization, separation of different evolutionary events, and straightforward operation without requirements for special culturing or monitoring equipment.

## Results

We began by inoculating M13 phages, which conduct chronic infections without lysing or severely damaging their host cells, (purple dot in Fig 1B) in front of a motile bacterial inoculum. A substantial fraction of the expanding cells in the front encountered phages and got infected, resulting in a slowdown of their subsequent growth (Appendix Fig S1). Progeny phages were then produced and carried forward along the expansion route by infecting neighboring fresh cells. This combination of cell migration and repeated phage infection cycles was expected to result in the formation of a visible fan-shaped infection zone with lower cell density than the uninfected regions (Li et al, 2020) (Fig 1B). Experiments showed that a suspension of exponentially growing *Escherichia coli* FM15 cells (Appendix Table S1), when inoculated at the center of an 8.5-cm Petri dish containing 10 ml of LB medium and 0.25% agar, formed a uniform bacterial lawn after overnight incubation (first row in Fig 1C). In contrast, inoculating bacteria at the center and  $10^3$  PFU of M13 phages 1 cm away from the center of an identical semisolid agar plate led to formation of a dark (low cell density) fan-shaped pattern in the midst of a white (high cell density) bacterial lawn after overnight incubation (second row in Fig 1C). The fan-shaped pattern of low cell density area was stable for days until the agar dried up.

To gain a quantitative understanding of the patterning process, we developed a mathematical model, RESIR (Range Expansion with Susceptible Infected Recovered kinetics) model derived from previous models (Kermack & McKendrick, 1927; Cremer et al, 2019), based on the characterized properties of the bacteria–phage interaction (Fig EV1A, Appendix Fig S2, Materials and Methods). In our model, numerical simulations with realistic parameter values (Appendix Table S2) recaptured the fan-shaped pattern as the experiments (bottom two rows in Fig 1C). The saturated cell density in this fan-shaped region is lower than that of uninfected region because the nutrient is partially consumed by phage production and is hence less available for supporting bacterial growth (Appendix Fig S3), thereby yielding a visible low cell density region. The development of the fan-shaped pattern was mainly driven by the expansion in the radial direction, supplemented by the extension in the lateral direction (Fig EV1B).

One prediction of the model was that, at the boundaries of the fan, uninfected cells migrating side by side with infected cells continuously served as fresh hosts for progeny phages during the range expansion, resulting in a moderately higher phage titer at the sideward edge than in the central region of the fan-shaped infection zone (Fig 1C and D). To verify this, we visualized the phage-infected bacteria by introducing a fluorescence gene accompanied with phage infection. Specifically, we constructed a reporter phage M13-GFP harboring a “superfolder” variant of green fluorescent protein (*gfp*) gene located downstream of gene *IV* in the wild-type M13 phage genome. The infection of M13-GFP phage introduces the *gfp* gene into the host bacteria. Thus, the bacteria infected by M13-GFP phage could be visualized by the fluorescent signal which reflects the expression level of phage genes locally (Fig 1E). As shown in Fig 1F and G, the brightest fluorescent signals in the semisolid agar plate, which suggested the highest cumulative expression of genes in the phage genome including *gfp*, overlapped with the sideward edge of the infection zone, consistent with the model simulation (Fig 1D).

The model simulation also predicted that the size of the fan-shaped pattern increased with the phage production rate (Fig EV1C). To test the proportionality predicted by the model, we borrowed one key design in PACE, an activity-dependent phage propagation module located in an accessory plasmid (Esvelt et al, 2011), which constructs a linkage between the function of the biomolecule to be evolved and phage propagation via the activation of *gIII* expression. It is known that the production of M13 phage scales with increasing levels of its minor coat protein pIII (encoded by *gIII*) over concentrations spanning two orders of magnitude (Rakonjac & Model, 1998). We used this design to vary the phage production rate by altering the expression level of *gIII*. Specifically, a selection phage (Esvelt et al, 2011) was constructed by replacing the intrinsic *gIII* of the M13 genome with the wild-type T7 RNA polymerase (RNAP) gene, while a copy of *gIII* was inserted into an accessory plasmid (Esvelt et al, 2011) in the host *E. coli* cell (Fig EV2A). The expression of *gIII* was put under the control of a library of 17 T7 promoter variants (Appendix Table S3), on which wild-type T7 RNAP exhibits different levels of activities ranging from 0.005 to 85% of the activity of wild-type T7 RNAP on the T7 promoter (Fig EV2B). When a high-copy-number accessory plasmid was used (Materials and Methods, Appendix Table S4), the area sizes of the fan-shaped pattern steadily increased with increasing expression levels of *gIII*, saturating at an activity level approximately 1.7% of the wild-type T7 RNAP activity on the T7 promoter (Fig EV2C). To distinguish more finely between high expression levels, a low-copy-number accessory plasmid was employed (Materials and Methods, Appendix Table S4). The combined utilization of the high- and low-copy-number accessory plasmids provided a measurement range of expression activity spanning 4 orders of magnitude (Fig EV2D). These results suggested that the area of the fan-shaped pattern could be used as a straightforward assessment of the activity of interest. We first used the high-copy-number accessory plasmid unless noted otherwise.

To develop our system of spatial directed evolution, we next sought to modulate the second key design in PACE, the mutagenesis plasmid (Badran & Liu, 2015; Bryson et al, 2017), to match the needs of the applications in semisolid media. The mutagenesis plasmid (MP4) typically used in PACE includes three mutators: DnaQ926, a dominant negative mutant of the delta domain of *E. coli* DNA polymerase, Dam, DNA adenine methyltransferase, and SeqA, a negative regulator of replication initiation (Badran & Liu, 2015). The expression of these mutator genes is driven by a small molecule inducer arabinose. Differently, for our spatial evolution system, we employed phage shock protein promoter ( $P_{psp}$ ) (Brissette et al, 1990, 1991) to drive the expression of the mutators upon M13 phage infection via a pIV-dependent signaling cascade (Brissette et al, 1991), generating the mutagenesis plasmid MP-s for this study (Appendix Table S4). The stringency of the  $P_{psp}$  was confirmed by using *E. coli* FM15 cells carrying a plasmid with *gfp* under the control of  $P_{psp}$  (Fig 2A). The cells exhibited green fluorescence only in the presence of phage infection (Fig 2B), confirming the stringency of this promoter could prevent undesired induction of mutagenesis in bacteria cells before they came into contact with phages. The mutation rate conferred by MP-s was measured to be comparable to that of MP4, which is  $4.4 \times 10^{-7}$  and approximately  $5.9 \times 10^{-4}$  substitutions per bp per generation for *E. coli* and M13 phage, respectively (Badran & Liu, 2015; Materials and Methods).

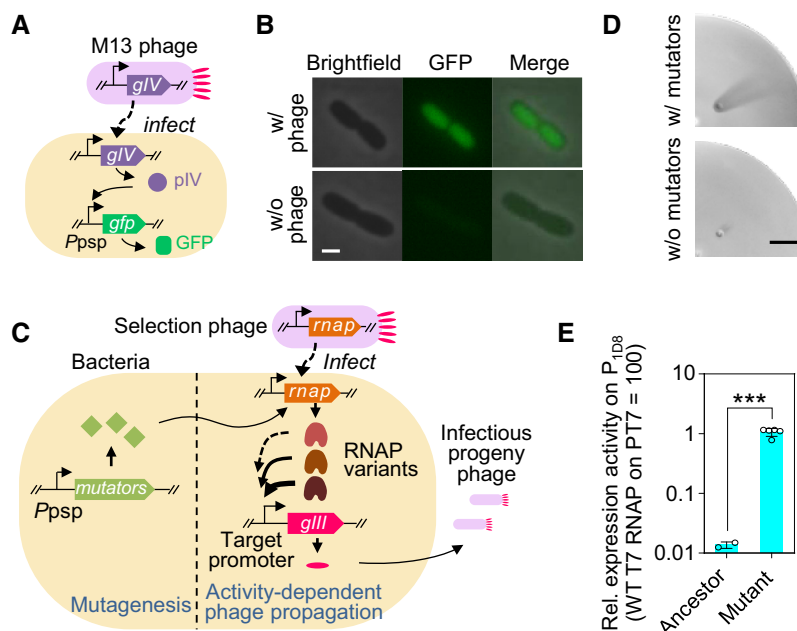


**Figure 2. Establishment of a prototypic SPACE system.**

- A Reporter system to verify phage infection-inducible expression of proteins conferred by the phage shock protein (psp) promoter via a pIV-dependent signaling cascade (Brissette et al, 1991). In the mutagenesis plasmid MP-s developed in this study, *gfp* was replaced with mutator genes (Badran & Liu, 2015).
- B Microscopic images of *E. coli* FM15 cells carrying a plasmid with *gfp* gene downstream of the *psp* promoter with or without wild-type M13 phage infection. Scale bar: 1  $\mu$ m.
- C Schematic design of SPACE coupling T7 RNAP activity with the expression of *gIII*. The host bacteria carry a mutagenesis module and an activity-dependent phage propagation module, which are harbored by the mutagenesis plasmid MP-s and the accessory plasmid, respectively.
- D Photographs of a quarter of the semisolid agar plate of a SPACE experiment using high-copy accessory plasmid to improve within-cell activity of T7 RNAP on a synthetic promoter 1D8. An *E. coli* FM15 strain carrying no MP was used as control. Scale bar: 1 cm.
- E Activity in cells of T7 RNAP and its mutants from the SPACE experiment in (D). Two clones of the ancestor and five clones of the mutants obtained from the evolution towards 1D8 recognition were measured by *in vivo* transcriptional assay (Materials and Methods). Two-tailed *t*-test was used to compare the two groups. \*\*\* $P = 0.0001$ . Data represent mean values  $\pm$  s.d.

Source data are available online for this figure.

By introduction of the accessory plasmid carrying the activity-dependent phage propagation module and MP-s carrying the *in vivo* mutagenesis module into our motile host strain, *E. coli* FM15, we established a prototypic system named as SPACE, standing for Spatial PACE. In SPACE, ancestor selection phages (Esvelt et al, 2011) carrying a wild-type T7 RNAP gene infect bacterial cells, and the expression of mutator genes induced by the infection leads to mutations in the RNAP gene during the replication of phage genome, and then expression of different RNAP variants. Desired RNAP variants with improved activity on the target synthetic promoter activate the expression of *gIII* on an accessory plasmid to produce infectious progeny phages, which in turn infect neighboring susceptible bacterial cells and repeat the process (Fig 2C). In contrast, RNAP variants that do not lead to sufficient production of pIII and infectious progeny result in the formation of typically much smaller fan-shaped pattern or no infection zone at all.

As an initial test of SPACE, T7 RNAP was evolved to recognize a synthetic promoter named 1D8 (Appendix Table S3) with nine bases different from wild-type T7 promoter. A distinct fan-shaped pattern was observed after 20 h development (upper panel of Fig 2D), while no infection zone was formed on the host cells lacking the mutagenesis module (lower panel in Fig 2D). From the sideward

edge of the fan-shaped pattern, five phage clones were purified. Their average transcriptional activity on the promoter 1D8 was 70-fold greater than that of the wild-type T7 RNAP (Fig 2E, Materials and Methods). These results established the ability of the SPACE system to evolve enzyme activities on a single agar plate with minimal efforts.

To better understand the underlying evolutionary process of the SPACE experiment, we extended the RESIR model to describe competitions between two phages with different progeny production rates. The simulated competition results in a spatial separation between the two phages, of which the strong phages with higher progeny production rate dominate outer area near the sideward edge of the infection zone, while the weak phages with lower progeny production rate are confined inside (Fig EV3A and B). To experimentally validate the spatial separation of phages, we competed a phage M13s carrying a red fluorescent protein (*rfp*) gene in wild-type M13 genome against a weaker variant (M13w) carrying a *gfp* gene (Fig 3A). M13w harbored three mutations K184A/R186A/D187A in its *gIII*, which resulted in lower progeny productivity than wild-type M13 (Deng & Perham, 2002). The expression of red or green fluorescent proteins induced by the infection of M13s or M13w could thereby indicate the spatial distribution of these two

phages (Fig 3B). Their spatial abundance patterns were characterized after 20 h of competition assay (Materials and Methods) with an initial titer ratio of 1:1 between M13w and M13s. As expected, M13s (red) dominated the outer area of the fan-shaped infection region along the direction of the sideward edges, while the M13w (green) was localized in the inner area mostly around the initial inoculation spot (Fig EV3C and D).

To more closely reflect actual evolutionary process, in which stronger phages may be generated at very low frequencies, we repeated the competition assay with an M13w: M13s inoculant ratio of  $10^5:1$ . Both experimental and theoretical results showed

that the strong phage M13s could eventually outcompete the weak and take over the population as the phage population spread via its range-expanding host (Fig 3C and D, Appendix Fig S4). And the strong phage is accumulated most efficiently at the sideward edge of the infection zone due to the most active infections occurring there. Thus, during SPACE process, the advantageous phage mutants with high production rates, which usually occur at very low frequencies in an evolutionary process, would be autonomously separated from the weaker and get enriched rapidly at the sideward edge of the infection zone, as illustrated in Fig 3E.

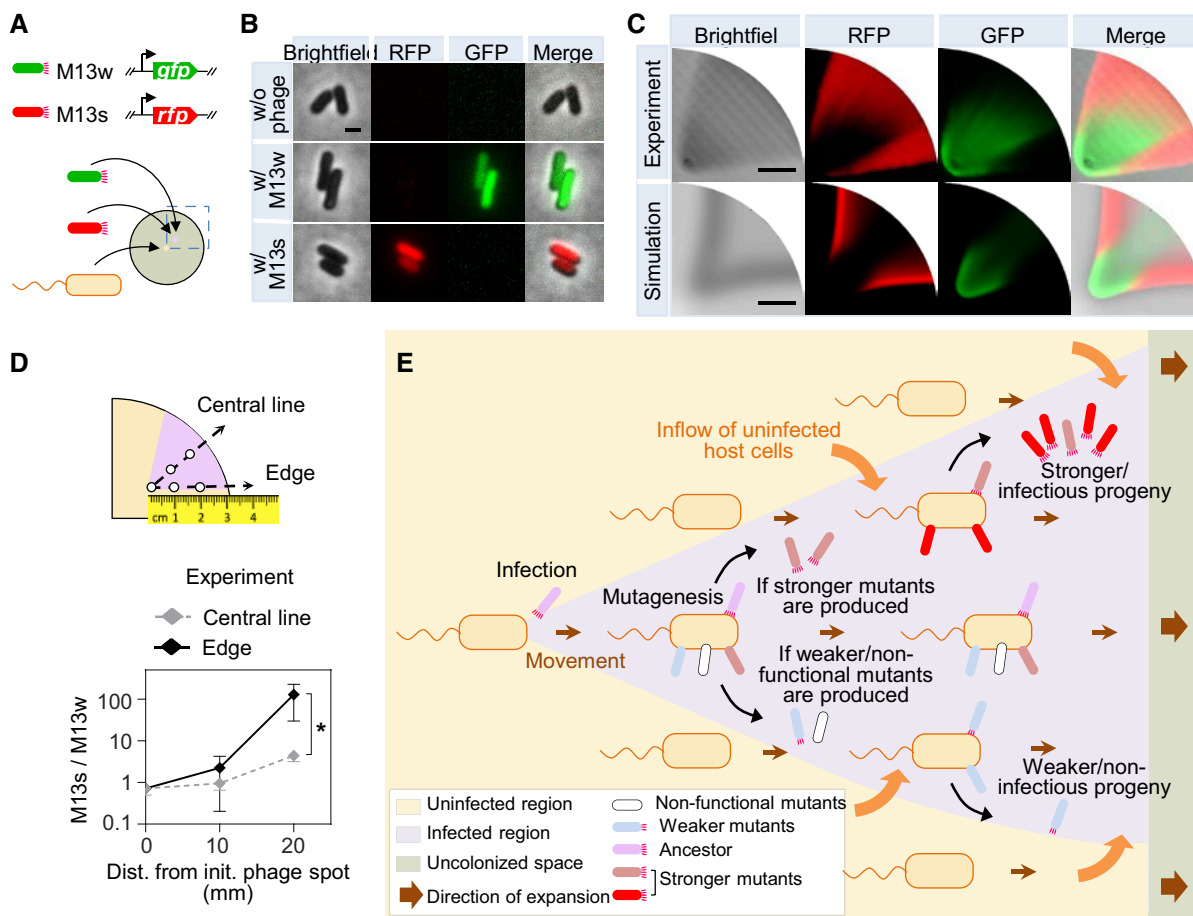


**Figure 3. Spatial competition and adaptation of phages during range expansion of their hosts.**

- A Design of a competition assay between phages with different production rates. M13s carries a red fluorescent protein (*rfp*) gene in a wild-type M13 genome, while a weaker phage variant M13w carries a green fluorescent protein (*gfp*) gene. The phage titers of M13s and M13w were  $9.6 \times 10^8$  and  $1.3 \times 10^7$  PFU/ml, respectively, after 2.5 h propagation in *E. coli* FM15 by shaking incubation at 37°C with a multiplicity of infection (MOI) of 0.001.
- B Microscopic images of *E. coli* FM15 cells with or without phage infection. Scale bar represents 1  $\mu$ m.
- C The experimental result shows raw photographs of a representative two-phage competition 20 h after initial inoculation with  $10^5:1$  mixture of M13w: M13s at 1 cm away from the center. The simulation result is the outcome of competition between two phages PW and PS with relative production rates of 40 and 100, respectively. Scale bar represents 1 cm.
- D Phage titer ratio of M13s to M13w along the central line and the edge of the fan-shaped infection zone in the experimental result in (C). Samples were collected from different positions as shown in the schematic and phage titer was quantified by qPCR (Materials and Methods). Data represent mean values  $\pm$  s.d. for three independent assays. Two-tailed *t*-test was used to compare two groups. \**P* = 0.028.
- E Illustration of the phage spatial evolution process during the range expansion of the host bacteria. Mutants with improved activity to produce infectious progeny phages continuously infect neighboring susceptible bacterial cells and get enriched along the sideward edge of the fan-shaped infected zone; meanwhile, weak mutants that do not lead to sufficient production of infectious progeny result in typically much smaller fan-shaped pattern or no visible infection region at all.

Source data are available online for this figure.

We next demonstrated that SPACE is scalable and parallelizable. Ninety-six SPACE experiments were carried out concurrently to evolve T7 RNAP to recognize a library of random T7 promoter variant sequences (Fig 4A). The starting selection phage carrying wild-type T7 RNAP was inoculated onto 96 semisolid agar plates, each of which contained an inoculum of host cells harboring an accessory plasmid containing a random T7 promoter variant (Appendix Table S3) and the mutagenesis plasmid MP-s. Twenty out of the 96 experiments were deemed as successful evolution based on the formation of the fan-shaped pattern, and the evolved phages were isolated and sequenced for mutations in the T7 RNAP mutants (Fig 4B). As the size of the fan-shaped pattern is linked to the activity of RNAP (Fig EV2), we compared the size of the infected region to assess the improvements in enzyme activity, and confirmed that the isolated mutant phages

presented larger fan-shaped patterns than the ancestor (Figs 4B and EV4A). The expression activity levels of the evolved RNAP mutants on their target sequences were further measured *in vivo* based on flow cytometry (Fig EV4B, Appendix Fig S5), and also calculated using the area-to-activity transfer function (given in Fig EV2D). Roughly consistent with the calculation, the fold change in measured activities of the RNAP mutants ranged from 8.1 (4A2) to 918.3 (1C12) as compared with the activity of wild-type T7 RNAP on the corresponding promoters (Fig EV4B). Several evolved T7 RNAP mutants were further purified and assayed *in vitro* (Materials and Methods), and the purified RNAP mutants exhibited improvements ranging from 3.4-fold (1G8) to 72.9-fold (1D8), compared with the starting enzyme (Fig 4C). Aside from mutations at frequently reported sites including E222, N748, Q758, D770, and E772 (Ikeda *et al*, 1993; Raskin *et al*, 1993; Rong *et al*,

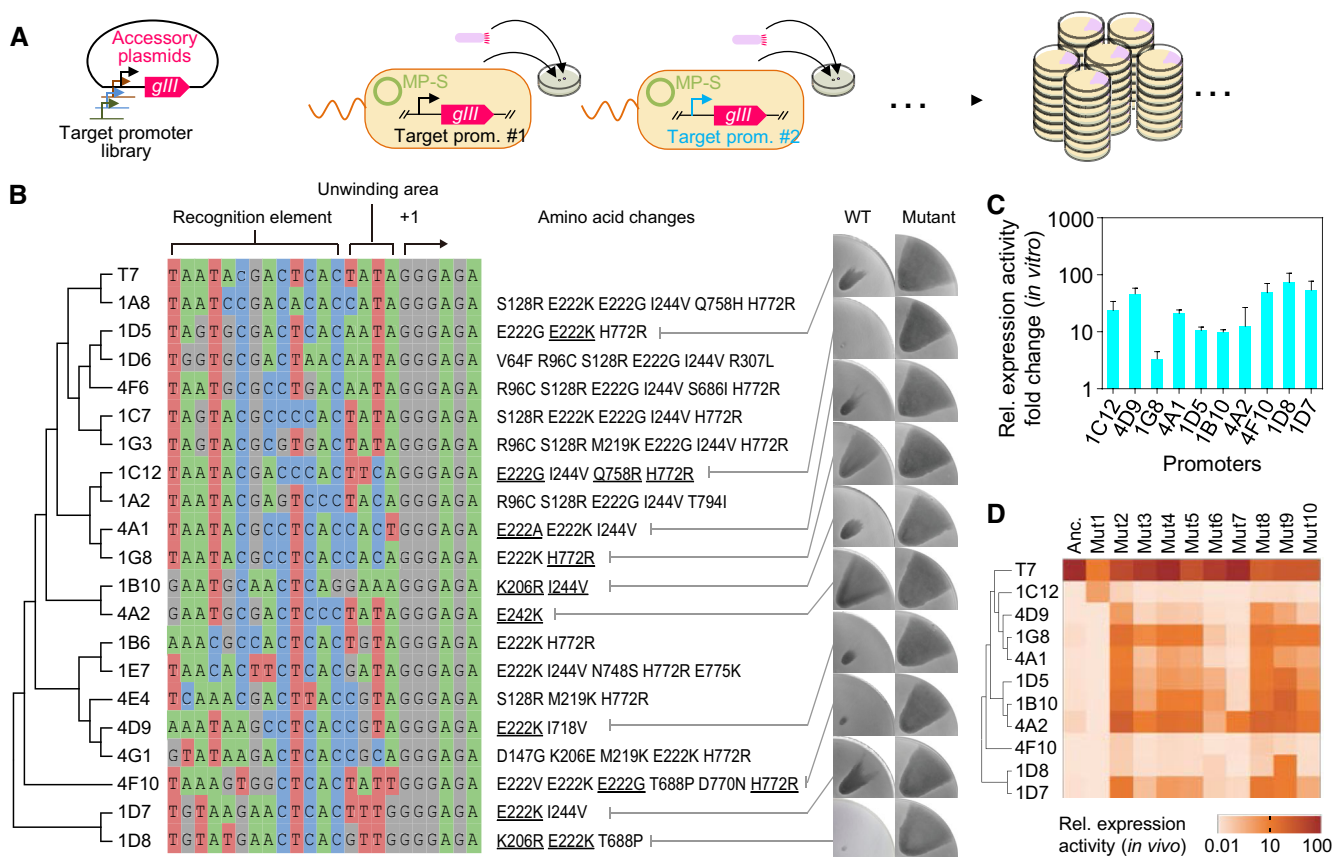


**Figure 4. Parallelizable SPACE system.**

- A** An illustration of the parallelized SPACE experiments. Each FM15 strain carrying an accessory plasmid with a specific target promoter on it was inoculated on an agar plate to launch the experiments in parallel.
- B** List of library promoter sequences for which SPACE produced improved RNAP variants relative to wild-type RNAP (wild-type T7 promoter sequence is at the top). For 10 selected promoters, improvement of RNAP performance is demonstrated visually on the right, by comparing the size of fan shapes formed by phages carrying corresponding mutant RNAP genes (underlined mutations) with those formed by ancestor (anc.) phages carrying the wild-type T7 RNAP gene. The images of a quarter of the agar plate containing a representative fan-shaped pattern are shown.
- C** Fold change in the relative expression activity of the evolved RNAP mutants as compared with the wild-type T7 RNAP, for the 10 selected promoter sequences corresponding to the images in (B). Results were obtained by *in vitro* transcriptional assay (Materials and Methods). Data represent mean values  $\pm$  s.d. for three biologically independent assays.
- D** Expression activity of 10 RNAP mutants on T7 promoter and 10 promoter variants measured by *in vivo* transcriptional assay. Mutants are arranged in the same order as their original target promoters listed on the left side of the heatmap. Amino acid changes of each mutant are listed in Appendix Table S5. Data are normalized so that the activity of wild-type RNAP on the T7 promoter is 100; the mean for three biologically independent replicates is shown (Materials and Methods).

Source data are available online for this figure.

al, 1998; Imburgio et al, 2000; Meyer et al, 2015), some new mutations such as I244V, K206E/R, M219K, and T688P were detected repeatedly. They might play important roles in the recognition of the corresponding artificial promoters, which needs further investigations.

To assess the orthogonality and promoter malleability of the evolved RNAP mutants, we generated an activity map based on the *in vivo* measurements of 11 promoters against 10 RNAP mutants (Fig 4D, Appendix Fig S6, Appendix Tables S3 and S5). All evolved RNAP mutants retained their activities on the T7 promoter. Besides wild-type T7 RNAP, Mut1 and Mut7 were orthogonal, recognizing only their target sequences (1C12 and 4A2, respectively) and the T7 promoter. Apart from these, off-target crosstalk is consistently observed between different pairs (Fig 4D), which needs further efforts to remove the promiscuity of these RNAPs if they are to be applied in genetic circuit design (Tabor, 2012). The mutation E222K, known to be a specificity broadener (Ikeda et al, 1993), led to nonspecific activity on almost all sequences tested. Aside from changing from glutamic acid to lysine, other mutations at the same site including E222A (mut5) and E222G (mut6) produced mutants with similar off-target activities. H772R (mut8) also showed some non-specific activity. However, combining E222G and H772R, with one more mutation Q758R, resulted in mut1, which, as described, is highly orthogonal. This implied an underlying epistatic phenomenon. Construction of an exhaustive activity map of RNAP mutants and random sequences would be of interest to deepen understanding of the origin of the orthogonality and promoter malleability. To this end, SPACE can be used to generate abundant mutants and assay the activity without additional infrastructure.

## Discussion

Range expansion is a widely observed phenomenon in nature, which involves the movement and successful establishment of natural populations across new territories due to biological invasion, anthropogenic habitat conversion, or changes of the abiotic and biotic environmental factors (Andow et al, 1990; Walther et al, 2002; Parmesan & Yohe, 2003; Hastings et al, 2004; Excoffier et al, 2009; Fronhofer & Altermatt, 2015; Gandhi et al, 2016; Ochocki & Miller, 2017; Ramirez et al, 2019; Aguirre-Liguori et al, 2021; Liu et al, 2021). Although nonmotile, nonlethal viruses can be easily transmitted via their host species conducting range expansion and therefore spread to broader territories (Jones, 2009; Kareinen et al, 2020). It has been assumed that movements of migrating animal species could enhance the spread of pathogens including zoonotic viruses posing severe threats to human health (Altizer et al, 2011). However, the mechanism by which the range expansion of host species influences the adaptation and evolution of their viruses remains to be elucidated.

It is recognized that range-expanding species experience active evolutionary changes at the expanding front (Deforet et al, 2019; Miller et al, 2020). The fast-dispersing individuals with superior moving ability outrun other individuals of the species and inevitably accumulate at the front, resulting in an evolutionary increase in the moving ability in successive generations. This process has been proposed as a new evolutionary mechanism called “spatial sorting” (Shine et al, 2011; Phillips & Perkins, 2019). Researchers also found that parasite that infects range-expanding hosts will itself be

subjected to spatial sorting (Shine et al, 2011), and its improved ability to successfully infect hosts is favored during this evolutionary process (Kelehear et al, 2012). Considering that viruses are obligate parasites and copropagate with their hosts, one could intuitively speculate that viruses that infect a range-expanding host will experience the same evolutionary process with the host, that is, the evolutionary changes of viruses mostly accumulating at the front of host expansion. However, our results in this study have proven otherwise. Unlike the spatial sorting of host species (Deforet et al, 2019; Miller et al, 2020), the active infection of neighboring susceptible host cells leads to the spatial sorting of phages with different progeny productivities perpendicular to the direction of host front propagation. Therefore, other than at the expanding front, bacteriophage genotypes associated with higher phage progeny production rate are significantly accumulated along the sideward edge of the fan-shaped infection zone. It can also serve as a null hypothesis for the prediction of viral spread and evolution during host range expansion for future ecological studies of higher organisms.

Moreover, we applied this ecological insight to develop a SPACE system. Unlike the 17 continuous directed evolution tools comprehensively summarized by a recent review (Morrison et al, 2020), our SPACE system introduces spatial dimensions into continuous directed evolution to streamline protein engineering. This remarkably reduces the complexity of the continuous directed evolution apparatus, and enables direct visual assessment of the progress of the evolution experiments through the link between phage production rate and the size of the infection zone. As to PACE system, its selection stringency has to be optimized from time to time to avoid complete phage washout. To accelerate the selection process, the flow control needs to be closely monitored, either by manually collecting samples from the lagoon and checking the intensity of reporter signals as well as the phage titer, or by using a specialized in-line monitoring instrument (Carlson et al, 2014; Badran et al, 2016), which limits the number of evolution experiments that can be performed in parallel. Moreover, PACE relies solely on the time scale to select for stronger phage mutants based on their faster reproduction in the well-mixed liquid system. In SPACE system, the stronger mutants are spontaneously separated from weaker ones through spatial competition and get most enriched at the rim end of the sideward edge of the fan-shaped infection region. In addition, our model also predicted that the fold-enrichment rate of beneficial mutants provided by the SPACE system is higher than the optimal rate that a chemostat-like liquid continuous culturing system could achieve, regardless of the detailed progeny production rates of the mutants (Appendix Fig S7). These features of SPACE provide convenience to enable evolutionary applications that require extensive parallelization with efficiency, and it is easy to implement in general biology laboratories without expensive automated robotic experimental systems (DeBenedictis et al, 2022).

We have demonstrated that SPACE could improve the *in vivo* transcriptional activity of T7 RNAP on an artificial promoter by 70-fold after a round of overnight experiment (~20 h), which is comparable to the ~100-fold increase in activity on P<sub>T3</sub> achieved by PACE at 28 h (Carlson et al, 2014). However, current format of SPACE system still has its drawbacks. For example, the selection stringency cannot be flexibly adjusted within one round of experiment, and the phage generations need to be increased by transferring evolved

phages to a fresh agar plate to start a new run (Appendix Text S1). As a future upgrade, additional relevant factors such as the concentrations of agar and chemoattractant in the media could be tuned to change the expansion speed of bacteria (Liu *et al*, 2019) and hence enable more flexible control over the selection stringency of the system. We expect that the increased expansion speed would result in higher selection stringency, meaning that mutants have to exhibit higher level of improvements in their activity to co-propagate with the range-expanding bacteria and outcompete other mutants (Appendix Fig S8). In addition, an attractive application of SPACE is to chart empirical fitness landscape by extensively parallelized evolution experiments. As the “fossils” will be left behind the expanding front in space, together with the convenient visual readout of competition outcomes, SPACE enables extensive exploration of fitness landscape. Overall, SPACE provides a powerful platform for applied research and fundamental investigation of evolutionary mechanisms.

## Materials and Methods

### Strains and media

DNA cloning was performed with chemically competent *E. coli* DH5 $\alpha$  cells (TransGen, Beijing). All plaque assays, bacterial migration tests, *in vivo* transcriptional assays, and SPACE experiments were performed using *E. coli* FM15 strain. This strain was derived from *E. coli* MG1655-mCherry (Liu *et al*, 2019) by the following steps: (i) rendered F<sup>+</sup> by conjugation with *E. coli* K12 ER2738 (NEB); (ii) deletion of the  $\alpha$ -fragment of LacZ gene with the  $\lambda$  Red recombining system. The genotype of the resulting strain FM15 is F<sup>+</sup> *proA* + B<sup>+</sup> *lacI<sup>q</sup>*  $\Delta$ (*lacZ*)M15 *zzf::Tn10* (*TetR*)/ $\lambda$ -*ilvG*-*rfb-50 rph-1 attB::Kan<sup>R</sup>*  $\Delta$ (*lacZ*)M15. Information about bacterial strains used in the study is listed in Appendix Table S1. Cells were cultured in Luria-Bertani medium (LB: 10 g/l NaCl, 10 g/l tryptone, 5 g/l yeast extract). LB containing 0.25% (w/v) agar (Huankai, Guangdong) was used for SPACE experiments. Antibiotics including chloramphenicol (25  $\mu$ g/ml), tetracycline (15  $\mu$ g/ml), carbenicillin (50  $\mu$ g/ml), and spectinomycin (100  $\mu$ g/ml) were added where appropriate. For *in vivo* transcriptional activity measurement, M9 medium (6.78 g/l Na<sub>2</sub>HPO<sub>4</sub>, 3 g/l KH<sub>2</sub>PO<sub>4</sub>, 1 g/l NH<sub>4</sub>Cl, 0.5 g/l NaCl) was used, with casamino acid (CAA) and glucose supplemented where necessary.

### Cloning and plasmid construction

The vectors were constructed with Gibson assembly (NEB) or ClonExpress II One Step Cloning (Vazyme, Nanjing) kits. PCRs were carried out with PrimeSTAR Max (Takara) or Q5 (NEB) following the manufacturers' instructions. Accessory plasmids (Esvelt *et al*, 2011) for T7 RNAP evolution contained, in order, an *rrmB* terminator, the promoter of interest, a strong RBS 5'-AAGGAGGAAAAAATATATAATG-3' where underlined bases represent the start codon, *gIII*, either the combination of *aadA* gene conferring spectinomycin resistance and pUC origin for a high-copy version or *bla* gene conferring carbenicillin resistance and SC101 origin for a low-copy version. Reporter plasmids were identical to SC101 accessory plasmids except for the replacement of *gIII* by *gfp*. T7 RNAP selection phage (Esvelt *et al*, 2011; Wu *et al*, 2021)

was constructed by replacing all but the last 202 bp of *gIII* with the gene encoding T7 RNAP in M13K07 (NEB) helper phage and then removing the p15a origin of replication and *aph* gene to restore the M13 origin of replication. The mutagenesis plasmid (Esvelt *et al*, 2011; Badran & Liu, 2015) contained *dnaQ926*, *dam*, and *seqA* under control of *psp* operon. Information about plasmids used in the study is listed in Appendix Table S4.

### Construction of promoter libraries

A target promoter library was constructed by altering bases of the original T7 promoter at positions from -17 to -1 relative to the transcriptional start site. In principle, this library should contain (4<sup>17</sup>-1) variants, which is not a reasonable size to subject to biological process. Therefore, several rules were applied to narrow down the sequences to those which are more likely to act as promoters: (i) G + C content within 40–60%; (ii) no complicated secondary structure nor self-complementary structure; (iii) no consecutive GC regions; (iv) classifiable according to sequence similarity to T7 promoter. After this step, the size of the promoter library was reduced to approximately 2000. Ninety-six promoters were randomly selected from this library for the SPACE experiments. The sequences of these promoters are listed Appendix Table S3. These promoters were inserted upstream of *gIII* in the accessory plasmids.

### Measurement of bacterial growth

The cells were grown according to the following protocol before assaying their growth curve. First, three single colonies of FM15 or FM15 carrying low-copy accessory plasmid with T7 promoter were picked from freshly streaked LB agar plates and grown overnight in 2 ml LB broth with appropriate antibiotics (tetracycline 15  $\mu$ g/ml, carbenicillin 50  $\mu$ g/ml) in Falcon tubes at 37°C with shaking (200 rpm). The overnight culture was then 1,000-fold diluted into prewarmed LB broth in Falcon tubes. After around 3-h shaking incubation when its optical density at 600 nm (OD<sub>600</sub>) reached 0.1–0.2, the diluted culture was again 20-fold diluted into prewarmed LB media in 100-ml flask and incubated for another 2 h. Then the OD<sub>600</sub> was measured with a Thermo Genesys 10S ultraviolet spectrophotometer and a proper volume of the culture was inoculated into 100 ml prewarmed LB to make an initial OD<sub>600</sub> of around 0.01 in 500-ml flasks. The flasks were then incubated in a Warm-bath Shaker (ZHICHU) maintained at 37°C and 200 rpm. When the OD<sub>600</sub> reached 0.1, bacterial suspensions were diluted to make OD<sub>600</sub> 0.01 and different quantities of M13 or SP-T7 phages were added into each flask to obtain final titers of 10<sup>7</sup> or 10<sup>8</sup> PFU/ml. The shaking incubation continued and samples were taken for measurement of phage titer and cell number every 10 min. The phage titers were calculated by double-layer plating plaque assay or by qPCR in a CFX Connect Real-Time System (BIO-RAD) using TB Green *Premix Ex Taq<sup>TM</sup>* II (Tli RNaseH Plus) (Takara) and primer sets: fg2 5'-GCTACAGCACCAGATTCAGC-3' and rg2 5'-AAGCAAACCTCAACAGG TCA-3' for all M13 phages; or SG2f 5'-CAATCGGTGATGGTCCTGT-3' and SG2r 5'-AACTCCAGCAGAACCATATGATC-3' for red fluorescence marker M13 phage. The cell numbers were assayed using a CytoFLEX flow cytometer (Beckman), and the gating strategy for this analysis was illustrated in Appendix Fig S5.



## Competition assay

GFP or RFP gene following a constitutive promoter J23100 was inserted into the phage genome downstream of *gIV*. Phages with different fluorescence genes were paired and mixed at titers ranging from  $10^3$  to  $10^9$  PFU/ml. Phage mixtures were made with different ratios dependent on experimental designs. FM15 cell suspensions at exponential phase ( $OD_{600} \approx 0.2$ ) and 2- $\mu$ l aliquots of the phage mixtures were inoculated onto soft agar. After 18–20 h incubation at 37°C, soft agar plates were inspected by fluorescence microscopy. When necessary, 2  $\mu$ l of the soft agar containing bacteria and phages was aspirated with a pipettor from different positions at the center or the edge of the fan-shape infection zone, added to 998  $\mu$ l fresh LB broth, and mixed by vortex at low speed. This liquid sample was then filtered through a 0.22- $\mu$ m pore size PES syringe filter to remove bacteria, and subjected to quantification of phage particles by qPCR.

## Single-cell fluorescence imaging

Fluorescence signals induced by M13s or M13w were measured after overnight co-culture of FM15 cells and phages in LB. For stringency test of *psp* promoter, FM15 cells carrying plasmid with/without *gfp* downstream of *P<sub>psp</sub>* were cultured until mid-log phase and subjected to M13 phage infection at a multiplicity of infection (MOI) of approximately 10 for 2 h. Cells were imaged using a Nikon Ti-E microscope equipped with a Plan Apo  $\lambda$  100 $\times$  Oil Ph3 DM objective (N.A. = 1.4) and an Andor Zyla 4.2 sCMOS camera. A 1% agarose pad with 0.9% NaCl was used to immobilize the cells. After cell immobilization, images were acquired within 5 min at room temperature (RT). Fluorescent images were taken with an EGFP filter (49002; ET470/40 $\times$ , ET525/50 m) or an RsRed filter (49005; ET545/30 $\times$ , ET620/60 m), and a 40-ms exposure time.

## Plate image capturing and processing

Plates were imaged using a Canon EOS 600D digital camera with a Canon EFS 18–135 mm lens and an exposure setting of f11, 1/500 s, ISO3200. The agar plates were illuminated by a white LED ring light with the diameter of 36 and 16 cm bellow (Liu et al, 2019). The area of fan shape was measured with ImageJ software (ver. 1.52a). For each plate, the region within a circle concentric to the plate bottom with radius 3.5 cm was used for area measurement.

Fluorescent images of agar plates with fan shapes were imaged using a Nikon Ti-E microscope and a Plan Fluor 4 $\times$  PhL DL objective (N.A. = 0.1). Each picture of a complete plate was obtained by stitching 27  $\times$  27 evenly divided square fields of view taken with the “ND processing” function of the NIS-Elements AR software (ver. 4.50.00). The green fluorescence images were taken with an EGFP filter (49002; ET470/40 $\times$ , ET525/50 m), and the red fluorescence with an RsRed filter (49005; ET545/30 $\times$ , ET620/60 m).

## Mutation rate measurement

M13mp18 (Messing, 1983) (NEB), a phage vector containing beta-galactosidase (*LacZ*) alpha gene (507 bp) downstream of *gIV* in the M13 genome, was used for the modified *lacZ* inactivation assay. Overnight cultures of *E. coli* FM15 without mutagenesis plasmid,

with *P<sub>psp</sub>*-driven mutagenesis plasmid MP-s constructed in this study, and with MP4 (Badran & Liu, 2015) used in PACE were inoculated into 2 ml LB media supplemented with antibiotics where appropriate, and cultured at 37°C until log phase ( $OD_{600} \approx 0.2$ ). Then approximately 20 PFU of M13mp18 was added to each bacterial culture. For induction of MP4, 25 mM (final concentration) of arabinose was added. The culture was continued to allow phages to propagate for 7–8 h. Supernatants containing progeny phages were collected after centrifugation and filtered through a 0.22  $\mu$ m pore-size PES syringe filter. These samples were serially diluted, mixed with 200  $\mu$ l log-phase culture of FM15 without mutagenesis plasmid, and applied to double-layered method with top agar containing 0.04% Blu-Gal (Sangon, Shanghai) and 15  $\mu$ g/ml tetracycline. The number of white or light blue plaques (*lacZ* $\alpha^-$  phenotype) and the total plaque number were counted and used as a measure of mutation frequency. After 24 h propagation on *E. coli* FM15 cells without mutagenesis plasmids, the testing phage vector did not produce any *lacZ* $\alpha^-$ -inactive mutant plaques, while 3.9 and 3.1% of mutant plaques were produced by phages propagated on FM15 carrying MP-s and MP4 (Badran & Liu, 2015), respectively.

## Range expansion-based continuous evolution

Soft LB agar was freshly prepared in 8.5-cm Petri dishes before each SPACE experiment. FM15 cells carrying both accessory plasmid and mutagenesis plasmid were cultured until its  $OD_{600} \approx 0.2$ , and 2- $\mu$ l aliquots of the cell suspension were inoculated at the center of the agar plates. Two microliters of selection phages with a titer of approximately  $5 \times 10^8$  PFU/ml were inoculated 1 cm away from the center of the soft agar. The inoculated plates were incubated at 37°C for 18–20 h, which was typically the duration of bacterial growth and phage propagation required for the formation of clear fan-shaped infection zone. After the incubation, 5  $\mu$ l of the soft agar containing bacteria and phages was aspirated with a pipettor from the end of each edge of the fan shape, added to 495  $\mu$ l fresh LB broth, and mixed by vortex at low speed. This liquid sample was then filtered through a 0.22- $\mu$ m pore size PES syringe filter to remove bacteria, and stored at  $-20^\circ\text{C}$  before use.

## In vivo transcriptional activity measurement

FM15 cells were grown according to the following protocol before assaying their fluorescence. First, cells were inoculated from three single colonies on LB agar plates and grown overnight in 2 ml LB or M9 supplemented with 1% (w/v) CAA and 0.4% (w/v) glucose with 15  $\mu$ g/ml tetracycline and 50  $\mu$ g/ml carbenicillin in Falcon tubes at 37°C with shaking (200 rpm). Then, the overnight cultures of *E. coli* FM15 carrying low-copy reporter plasmids containing *gIII* downstream of T7 promoter or T7 promoter variants were diluted 1,000-fold in prewarmed M9 supplemented with 1% CAA and 0.4% glucose in Falcon tubes. After approximately 3 h, once the diluted cultures reached an  $OD_{600}$  of 0.1–0.2, the cultures were diluted 20-fold with prewarmed media in Falcon tubes again and incubated for another 2 h.  $OD_{600}$  was measured with Thermo Genesys 10S ultraviolet spectrophotometer and cultures were diluted with prewarmed media to  $OD_{600}$  of 0.02 then divided into a 96-well plate. Selection phages carrying wild-type or mutant RNAP genes were prepared by adjusting phage titers to approximately  $10^{10}$  PFU/ml, and 20- $\mu$ l

aliquots were also added to make up a total volume of 200  $\mu$ l per well. The plate was then incubated at 37°C in a Digital Thermostatic Shaker (AOSHENG) maintained at 37°C and 1,000 rpm. Finally, after the 2-h incubation, a 10–20  $\mu$ l sample of each culture was transferred to a new plate containing 180–190  $\mu$ l PBS buffer and 2 mg/ml kanamycin to stop protein expression. For fluorescent protein maturation, all the samples were then incubated at 37°C in a Digital Thermostatic Shaker (AOSHENG) maintained at 37°C and 1,000 rpm for another 30 min. The fluorescence distribution of particles in each sample was assayed using a CytoFLEX flow cytometer (Beckman) with appropriate voltage settings (SSC: 500, FSC: 500, FITC: 2000); each distribution contained no < 50,000 events and was gated by the forward and side scattering using CytExpert (v2.2). The gating strategy for this analysis was illustrated in Appendix Fig S5. The intensity of fluorescence of each sample was calculated and normalized by the value of the wild-type T7 RNAP and T7 promoter pair.

### T7 RNAP purification

T7 RNAP and mutants were cloned into isopropylthio- $\beta$ -galactoside (IPTG) inducible expression vector, pQE82L, and transformed into *E. coli* BL21 competent cells. Clones were cultured in 5 ml LB with carbenicillin (50  $\mu$ g/ml) overnight and transferred into 200 ml fresh LB with carbenicillin and grown until  $OD_{600} \approx 1.2$ . Cells were then induced by IPTG (final conc. 0.5 mM) and incubated for another 3 h in a shaking incubator at 30°C. For cell lysis, the bacterial suspension was divided into 50-ml aliquots and centrifuged at the maximum speed at 4°C for 15 min. With supernatants removed carefully, pellets were resuspended in equal volume of lysis buffer (50 mM  $NaH_2PO_4$  pH 8.0, 300 mM NaCl, 0.5 mg/ml lysozyme, 0.5 mM dithiothreitol, DTT), and stored in freezer at –80°C immediately. After the samples were completely frozen (approximately 30 min), they were thawed on ice for 1 h, and this freeze–thaw cycle was repeated twice. The supernatants of bacterial lysates were collected by centrifugation and sterilized with 0.45  $\mu$ m pore-sized filters. Ni-sepharose columns were balanced with 10-fold volume of elution buffer (50 mM  $NaH_2PO_4$ , 300 mM NaCl, pH 8.0). Then the lysate supernatants were loaded onto each column and kept steady until all liquids passed through the column. Columns were washed with 5 ml of elution buffer containing 20  $\mu$ M imidazole, and then eluted with 5 ml elution buffer containing 20 and 50  $\mu$ M imidazole. Elutes were collected with 1.5-ml microtubes. Proteins were dialyzed in 100 mM NaCl, 50 mM Tris–HCl, 0.1 mM DTT, 0.1 mM EDTA, 50% v/v glycerol, pH 8.0, and stored at –20°C.

### In vitro transcriptional assay

The concentrations of purified T7 RNAP and mutants were determined by Bradford assay and then by Coomassie stain on a 10% SDS-PAGE gel. A 1.8-kb DNA fragment containing each promoter variant was amplified by PCR from the corresponding accessory plasmid. PCR products were purified with a QIAquick PCR purification kit, digested with *DpnI* to remove the template plasmids, and purified again. The purified amplicons were used as templates of the *in vitro* transcriptional assay. Transcription reactions with volume of 10  $\mu$ l consisted of 40 mM Tris–HCl (pH 7.9), 6 mM  $MgCl_2$ , 2 mM spermidine, 10 mM of DTT, 200  $\mu$ M of ribonucleotide tri-

phosphates, 0.3  $\mu$ l of RNase inhibitor, 0.2  $\mu$ l of pyrophosphatase, 1  $\mu$ M of T7 RNAP or mutant, 20 ng/ $\mu$ l template, and DEPC-treated water. Reactions were incubated at 37°C for 1 h, mixed with an equivalent volume of RNA loading dye consisting of 95% formamide, 0.02% SDS, 0.02% bromophenol blue, 0.01% xylene cyanol, and 0.5 mM EDTA, and then electrophoresed on 2% agarose gels. Gels were stained with 1  $\mu$ g/ml ethidium bromide and viewed on a UV transilluminator. Bands corresponding to transcription products were quantified with ImageJ software.

### Model for range expansion with susceptible infected recovered kinetics

Based on classic assumptions (Kermack & McKendrick, 1927; Bailey, 1957; Anderson & May, 1991; Busenberg & Cooke, 1993; Capasso, 1993; Hethcote, 2000; Keeling & Rohani, 2007), the host population could be categorized into three classes: the susceptible cells S, the infective cells I, and the recovered cells R. Susceptible cells enter into the infective compartment after catching an illness or virus and then into the recovered class as a consequence of recovery. Presumably, an individual who recovers from the illness has perpetual immunity thereafter. The model on the bases of these hypotheses is referred to as the SIR model, which is a classical and simple model to explain the rapid rise and fall in the number of infected patients observed in epidemics such as the plague (London 1665–1666, Bombay 1906) and cholera (London 1865).

Unlike most phages, the infection of M13 phage is chronic. During the process, infected host cells are not killed, and progeny phages are continuously produced and extruded through the cell membrane as the infected cells continue to grow at a lowered rate (Marvin & Hohn, 1969; Smeal *et al.*, 2017a, 2017b) until they become recovered (Appendix Fig S1). Recovered cells grow as fast as the susceptible ones, and they produce progeny phages at a much lower level as compared to the freshly infected cells (Appendix Fig S1). These features make it suitable to describe M13 phage infection process with a modified SIR model (Fig EV1, Appendix Fig S2). And different from models developed for other phages with a lytic life cycle, our model does not include a term of latent phase. This is because the initial period of ~10 min before the progeny phages start to be continuously produced (Marvin & Hohn, 1969; Ploss & Kuhn, 2010) is a negligible short time scale compared to the whole process of bacteria–phage copropagation (> 10 h) in our system.

For *E. coli* grown in semisolid agar plate, which allows the bacterial cells to swim, the spatiotemporal dynamics is governed by two elements: cell motility and cell growth, that is, diffusion, chemotaxis, and cell growth. To gain a quantitative insight on the spatial bacteria–phage copropagation process, we developed a RESIR (Range Expansion with Susceptible Infected Recovered kinetics) model based on navigated range expansion model of bacterial population (Cremer *et al.*, 2019) and modified SIR model of phage infection. The motility and chemotaxis of bacteria are represented by the Keller–Segel-type diffusion and advective terms widely used in the literature (Keller & Segel, 1971a, 1971b; Fu *et al.*, 2018; Cremer *et al.*, 2019). The spatiotemporal dynamics of bacterial cell density (susceptible bacteria S, infected bacteria I, recovered bacteria R), concentrations of the main nutrient (n) and chemoattractant (a), and the number of M13 phage particles (p) are described as follows:

$$\frac{\partial S}{\partial t} = \mu \nabla^2 S - \chi \nabla \cdot (S \nabla f) + \lambda(n)S - \kappa(p)\lambda(n)pS \quad (1)$$

$$\frac{\partial I}{\partial t} = \mu \nabla^2 I - \chi \nabla \cdot (I \nabla f) + \eta_1 \lambda(n)I + \kappa(p)\lambda(n)pS - \theta_1 I \quad (2)$$

$$\frac{\partial R}{\partial t} = \mu \nabla^2 R - \chi \nabla \cdot (R \nabla f) + \beta_1 \lambda(n)R + \theta_1 I \quad (3)$$

$$\frac{\partial n}{\partial t} = D_n \nabla^2 n - \lambda(n)(S + I + R)/Y_n \quad (4)$$

$$\frac{\partial a}{\partial t} = D_a \nabla^2 a - \gamma(a)(S + I + R) \quad (5)$$

$$\frac{\partial p}{\partial t} = \alpha[(1 - \eta_1)\lambda(n)I + (1 - \beta_1)\lambda(n)R] \quad (6)$$

Herein,  $\mu$  and  $\chi$  are the effective diffusion and chemotactic coefficient of bacteria, respectively;  $D_n$  and  $D_a$  are diffusion coefficients of the nutrient and chemoattractant, respectively.  $\eta_1$  and  $\beta_1$  are the growth suspension rate of infected bacteria and recovered bacteria,  $\theta_1$  is the recovery rate of infected bacteria,  $\alpha$  is the production rate of phage,  $Y_n$  is the yield nutrient consumption.

Chemotactic movement of bacteria depends on the concentration of the local attractant as follows (Liu *et al*, 2019):

$$f = \log \frac{1 + a/K_1}{1 + a/K_2} \quad (7)$$

where  $K_1$  and  $K_2$  are the lower and upper Weber offset of attractant sensing.

Bacterial cell growth is described with consideration of the growth limitations caused by nutrient availability (Murray, 2002), and follows a Monod relation

$$\lambda(n) = \frac{\lambda_0 n}{n + n_k} \quad (8)$$

with the Monod constant  $n_k$  and the growth rate  $\lambda_0$ .

Similarly, phage infection efficiency is described by a Monod relation

$$\kappa(p) = \frac{\kappa_0 p}{p + p_k} \quad (9)$$

with the Monod constant  $p_k$  and the phage infection efficiency  $\kappa_0$ .

In the same way, chemoattractant uptake is described by a Monod relation (Fu *et al*, 2018; Cremer *et al*, 2019):

$$\gamma(s) = \frac{g_0 a}{a + a_k} \quad (10)$$

with the Monod constant  $a_k$  and the uptake rate of chemoattractant  $g_0$ .

## Simulations

The equations of the above bacteria–phage interaction models were integrated in MATLAB (R2019a) using second-order-centered

differences for the spatial derivatives (mesh size 100  $\mu\text{m}$ ) and an explicit fourth-order Runge–Kutta routine for temporal integration (time step 1 s) in a Cartesian coordinate system. The parameters used in this study are summarized in Appendix Table S2.

Boundary conditions obey zero diffusive ( $\partial_x \Phi = 0$ ,  $\partial_y \Phi = 0$ , where  $\Phi = S, I, R, n, a, p$ ). The simulation starts with a locally restricted susceptible cell density  $S^{\text{init}}$ , in the radial distance  $r$  ( $r < 2$  mm) from the center of the simulation region,  $S^{\text{init}} = S_0 e^{-\frac{r^2}{r_0^2}}$  ( $S_0 = 0.2$  OD<sub>600</sub> and  $r_0 = 1$  mm), and the initial phage density at the inoculated site is  $p^{\text{init}} = p_0 e^{-\frac{r^2}{r_0^2}}$ , where  $r_0 = 1$  mm, and  $p_0 = 1$  a.u. The initial nutrient and attractant concentrations are homogeneously distributed with the concentration  $n_0 = 30$  mM and  $a_0 = 60$   $\mu\text{M}$ .

## Competition simulation

We further extended the RESIR model to the phage competitive model that can describe the competition between two phages, in which the phages were assumed to infect with different progeny phage production rates, despite the same infection efficiency. The phage competition infection efficiency is described as

$$\kappa(P) = \frac{\kappa_0(P_1 + P_2)}{(P_1 + P_2) + p_k} \quad (11)$$

The boundary conditions are the same as the former model, that is, all terms obey zero diffusive flux. The bacteria cell, nutrition, and chemoattractant initial conditions are the same as the former model, except for the phage. For initial conditions of the phage, the unequal (or equal) initial uniform mixture of two phages is located at the same position and the same initial density profile as the former model, that is,  $p_1^{\text{init}} = p_0 e^{-\frac{r^2}{r_0^2}}$  and  $p_2^{\text{init}} = C p_0 e^{-\frac{r^2}{r_0^2}}$ ,  $C$  representing the ratio of strong and weak phages in the initial mixture.

We further considered the possibility that resistant bacterial cells immune to phage infection at all times exist in the population. Experimental results showed that ~90% of the bacterial cells exhibit fluorescence signals 10 h after infection by a reporter phage carrying red fluorescent protein gene in its genome, and this percentage could maintain over an extended culturing period (Appendix Fig S9A). Subsequent transfer of such preinfected (recovered) cells into fresh medium and inoculation of another reporter phage carrying green fluorescent protein gene did not produce any cells exhibiting green fluorescence signals (Appendix Fig S9B). These results suggested that at least 90% of bacterial cells were infected and then became resistant, and this percentage could be maintained over time. The rest 10% were possibly immune to phage infection for unknown reasons even before exposure to phages. Nevertheless, even when we assume that 10% of the bacterial cells are indeed resistant to phage infection at the beginning, the conclusions of the model simulated phage spatial competition are not changed (Appendix Fig S10).

## Data availability

Major data for figures have been included in Source Data. Modeling and analysis code have been submitted to GitHub with a link <https://github.com/YiZhangsiat/RESIR-model>.

**Expanded View** for this article is available [online](#).

## Acknowledgements

The authors thank David R. Liu for insightful discussions and providing the plasmids which were used for the construction of accessory plasmid and mutagenesis plasmid. We thank Hui Wu for assistance with the protein analyses. This work was financially supported by Strategic Priority Research Program of Chinese Academy of Sciences (XDB29050500), National Key R&D Program of China (2018YFA0902700, 2018YFA0903600), National Natural Science Foundation of China (32025022, 32071417), Joint NSFC-ISF Research Grant (32061143021), CAS Interdisciplinary Innovation Team (Grant No. JCTD-2019-16), Shenzhen Science and Technology Innovation Committee (Grant No. JCYJ20180507182241844), Guangdong Provincial Key Laboratory of Synthetic Genomics (Grant No. 2019B030301006), and Guangdong Basic and Applied Basic Research Foundation (Grant No. 2020A1515110287).

## Author contributions

**Ting Wei:** Data curation; investigation; methodology; writing – original draft; writing – review and editing. **Wangsheng Lai:** Data curation; investigation; methodology; writing – original draft. **Qian Chen:** Data curation; investigation; methodology; writing – original draft. **Yi Zhang:** Software; methodology; writing – original draft. **Chenjian Sun:** Data curation; investigation; writing – original draft. **Xiongfei He:** Writing – review and editing. **Guoping Zhao:** Writing – review and editing. **Xiongfei Fu:** Software; supervision; methodology; writing – review and editing. **Chenli Liu:** Conceptualization; supervision; methodology; writing – original draft; project administration; writing – review and editing.

## Disclosure and competing interests statement

The authors have filed a provisional patent application on the SPACE system and related improvements.

## References

- Agresti JJ, Antipov E, Abate AR, Ahn K, Rowat AC, Baret J-C, Marquez M, Klibanov AM, Griffiths AD, Weitz DA (2010) Ultrahigh-throughput screening in drop-based microfluidics for directed evolution. *Proc Natl Acad Sci USA* 107: 4004–4009
- Aguirre-Liguori JA, Ramirez-Barahona S, Gaut BS (2021) The evolutionary genomics of species' responses to climate change. *Nat Ecol Evol* 5: 1350–1360
- Altizer S, Bartel R, Han BA (2011) Animal migration and infectious disease risk. *Science* 331: 296–302
- Anderson RM, May RM (1991) *Infectious diseases of humans: dynamics and control*. Oxford: Oxford University Press
- Andow DA, Kareiva PM, Levin SA, Okubo A (1990) Spread of invading organisms. *Landsc Ecol* 4: 177–188
- Badran AH, Liu DR (2015) Development of potent *in vivo* mutagenesis plasmids with broad mutational spectra. *Nat Commun* 6: 8425
- Badran AH, Guzov VM, Huai Q, Kemp MM, Vishwanath P, Kain W, Nance AM, Evdokimov A, Moshiri F, Turner KH et al (2016) Continuous evolution of bacillus thuringiensis toxins overcomes insect resistance. *Nature* 533: 58–63
- Bailey NTJ (1957) *The mathematical theory of epidemics*. London: Charles Griffin & Company
- Baym M, Lieberman TD, Kelsic ED, Chait R, Gross R, Yelin I, Kishony R (2016) Spatiotemporal microbial evolution on antibiotic landscapes. *Science* 353: 1147–1151
- Bloom JD, Arnold FH (2009) In the light of directed evolution: pathways of adaptive protein evolution. *Proc Natl Acad Sci USA* 106: 9995–10000
- Blum TR, Liu H, Packer MS, Xiong X, Lee P-G, Zhang S, Richter M, Minasov G, Satchell KJF, Dong M et al (2021) Phage-assisted evolution of botulinum neurotoxin proteases with reprogrammed specificity. *Science* 371: 803–810
- Bosshard L, Dupanloup I, Tenaille O, Bruggmann R, Ackermann M, Peischl S, Excoffier L (2017) Accumulation of deleterious mutations during bacterial range expansions. *Genetics* 207: 669–684
- Brisette JL, Russel M, Weiner L, Model P (1990) Phage shock protein, a stress protein of *Escherichia coli*. *Proc Natl Acad Sci USA* 87: 862–866
- Brisette JL, Weiner L, Ripmaster TL, Model P (1991) Characterization and sequence of the *Escherichia coli* stress-induced *psp* operon. *J Mol Biol* 220: 35–48
- Bryson DI, Fan C, Guo LT, Miller C, Soll D, Liu DR (2017) Continuous directed evolution of aminoacyl-tRNA synthetases. *Nat Chem Biol* 13: 1253–1260
- Busenberg SN, Cooke KL (1993) *Vertically transmitted diseases: models and dynamics*. Berlin, Heidelberg: Springer
- Capasso V (1993) *Mathematical structures of epidemic systems*. Berlin, Heidelberg: Springer
- Carlson JC, Badran AH, Guggiana-Nilo DA, Liu DR (2014) Negative selection and stringency modulation in phage-assisted continuous evolution. *Nat Chem Biol* 10: 216–222
- Chory EJ, Gretton DW, DeBenedictis EA, Esvelt KM (2021) Enabling high-throughput biology with flexible open-source automation. *Mol Syst Biol* 17: e9942
- Cremer J, Honda T, Tang Y, Wong-Ng J, Vergassola M, Hwa T (2019) Chemotaxis as a navigation strategy to boost range expansion. *Nature* 575: 658–663
- Crook N, Abatemarco J, Sun J, Wagner JM, Schmitz A, Alper HS (2016) *In vivo* continuous evolution of genes and pathways in yeast. *Nat Commun* 7: 13051
- DeBenedictis EA, Chory EJ, Gretton DW, Wang B, Golas S, Esvelt KM (2022) Systematic molecular evolution enables robust biomolecule discovery. *Nat Methods* 19: 55–64
- Deforet M, Carmona-Fontaine C, Korolev KS, Xavier JB (2019) Evolution at the edge of expanding populations. *Am Nat* 194: 291–305
- Deng L-W, Perham RN (2002) Delineating the site of interaction on the pIII protein of filamentous bacteriophage fd with the F-pilus of *Escherichia coli*. *J Mol Biol* 319: 603–614
- Dickinson BC, Packer MS, Badran AH, Liu DR (2014) A system for the continuous directed evolution of proteases rapidly reveals drug-resistance mutations. *Nat Commun* 5: 5352
- d'Oelsnitz S, Ellington A (2018) Continuous directed evolution for strain and protein engineering. *Curr Opin Biotechnol* 53: 158–163
- English JG, Olsen RHJ, Lansu K, Patel M, White K, Cockrell AS, Singh D, Strachan RT, Wacker D, Roth BL (2019) VEGAS as a platform for facile directed evolution in mammalian cells. *Cell* 178: 748–761
- Esvelt KM, Carlson JC, Liu DR (2011) A system for the continuous directed evolution of biomolecules. *Nature* 472: 499–503
- Excoffier L, Foll M, Petit RJ (2009) Genetic consequences of range expansions. *Annu Rev Ecol Evol Syst* 40: 481–501
- Fallah-Araghi A, Baret J-C, Ryckelynck M, Griffiths AD (2012) A completely *in vitro* ultrahigh-throughput droplet-based microfluidic screening system for protein engineering and directed evolution. *Lab Chip* 12: 882–891
- Fraebel DT, Mickalide H, Schnitkey D, Merritt J, Kuhlman TE, Kuehn S (2017) Environment determines evolutionary trajectory in a constrained phenotypic space. *Elife* 6: e24669

- Fronhofer EA, Altermatt F (2015) Eco-evolutionary feedbacks during experimental range expansions. *Nat Commun* 6: 6844
- Fu X, Kato S, Long J, Mattingly HH, He C, Vural DC, Zucker SW, Emonet T (2018) Spatial self-organization resolves conflicts between individuality and collective migration. *Nat Commun* 9: 2177
- Gandhi SR, Yurtsev EA, Korolev KS, Gore J (2016) Range expansions transition from pulled to pushed waves as growth becomes more cooperative in an experimental microbial population. *Proc Natl Acad Sci USA* 113: 6922–6927
- Harms MJ, Thornton JW (2013) Evolutionary biochemistry: revealing the historical and physical causes of protein properties. *Nat Rev Genet* 14: 559–571
- Hastings A, Cuddington K, Davies KF, Dugaw CJ, Elmendorf S, Freestone A, Harrison S, Holland M, Lambrinos J, Malvadkar U et al (2004) The spatial spread of invasions: new developments in theory and evidence. *Ecol Lett* 8: 91–101
- Hethcote HW (2000) The mathematics of infectious diseases. *SIAM Rev* 42: 599–653
- Hu JH, Miller SM, Geurts MH, Tang W, Chen L, Sun N, Zeina CM, Gao X, Rees HA, Lin Z et al (2018) Evolved Cas9 variants with broad PAM compatibility and high DNA specificity. *Nature* 556: 57–63
- Hubbard BP, Badran AH, Zuris JA, Guilinger JP, Davis KM, Chen L, Tsai SQ, Sander JD, Joung JK, Liu DR (2015) Continuous directed evolution of DNA-binding proteins to improve TALEN specificity. *Nat Methods* 12: 939–942
- Ikeda RA, Chang LL, Warshamana GS (1993) Selection and characterization of a mutant T7 RNA polymerase that recognizes an expanded range of T7 promoter-like sequences. *Biochemistry* 32: 9115–9124
- Imburgio D, Rong M, Ma K, McAllister WT (2000) Studies of promoter recognition and start site selection by T7 RNA polymerase using a comprehensive collection of promoter variants. *Biochemistry* 39: 10419–10430
- Jones RA (2009) Plant virus emergence and evolution: origins, new encounter scenarios, factors driving emergence, effects of changing world conditions, and prospects for control. *Virus Res* 141: 113–130
- Kareinen L, Ogola J, Kivisto I, Smura T, Aaltonen K, Jaaskelainen AJ, Kibiwot S, Masika MM, Nyaga P, Mwaengo D et al (2020) Range expansion of bombali virus in mops condylurus bats, Kenya, 2019. *Emerg Infect Dis* 26: 3007–3010
- Keeling MJ, Rohani P (2007) *Modeling infectious diseases in humans and animals*. Princeton, NJ: Princeton University Press
- Kelehear C, Brown GP, Shine R (2012) Rapid evolution of parasite life history traits on an expanding range-edge. *Ecol Lett* 15: 329–337
- Keller EF, Segel LA (1971a) Model for chemotaxis. *J Theor Biol* 30: 225–234
- Keller EF, Segel LA (1971b) Traveling bands of chemotactic bacteria: a theoretical analysis. *J Theor Biol* 30: 235–248
- Kermack WO, McKendrick AG (1927) A contribution to the mathematical theory of epidemics. *Proc R Soc Lond Ser A Contain Pap Math Phys Character* 115: 700–721
- Koster DA, Mayo A, Bren A, Alon U (2012) Surface growth of a motile bacterial population resembles growth in a chemostat. *J Mol Biol* 424: 180–191
- Li X, Gonzalez F, Esteves N, Scharf BE, Chen J (2020) Formation of phage lysis patterns and implications on co-propagation of phages and motile host bacteria. *PLoS Comput Biol* 16: e1007236
- Liu W, Cremer J, Li D, Hwa T, Liu C (2019) An evolutionarily stable strategy to colonize spatially extended habitats. *Nature* 575: 664–668
- Liu W, Tokuyasu TA, Fu X, Liu C (2021) The spatial organization of microbial communities during range expansion. *Curr Opin Microbiol* 63: 109–116
- Marvin DA, Hohn B (1969) Filamentous bacterial viruses. *Bacteriol Rev* 33: 172–209
- Messing J (1983) [2] New M13 vectors for cloning. In *Methods in Enzymology*, Wu R, Grossman L, Moldave K (eds), pp 20–78. San Diego, CA: Academic Press
- Meyer AJ, Ellefson JW, Ellington AD (2015) Directed evolution of a panel of orthogonal T7 RNA polymerase variants for *in vivo* or *in vitro* synthetic circuitry. *ACS Synth Biol* 4: 1070–1076
- Miller TEX, Angert AL, Brown CD, Lee-Yaw JA, Lewis M, Lutscher F, Marculis NG, Melbourne BA, Shaw AK, Szűcs M et al (2020) Eco-evolutionary dynamics of range expansion. *Ecology* 101: e03139
- Morrison MS, Podracky CJ, Liu DR (2020) The developing toolkit of continuous directed evolution. *Nat Chem Biol* 16: 610–619
- Murray JD (2002) *Mathematical biology I. An introduction*. New York, NY: Springer-Verlag
- Ni B, Ghosh B, Paldy FS, Colin R, Heimerl T, Sourjik V (2017) Evolutionary remodeling of bacterial motility checkpoint control. *Cell Rep* 18: 866–877
- Ochocki BM, Miller TE (2017) Rapid evolution of dispersal ability makes biological invasions faster and more variable. *Nat Commun* 8: 14315
- Packer MS, Rees HA, Liu DR (2017) Phage-assisted continuous evolution of proteases with altered substrate specificity. *Nat Commun* 8: 956
- Parmesan C, Yohe G (2003) A globally coherent fingerprint of climate change impacts across natural systems. *Nature* 421: 37–42
- Pham HL, Wong A, Chua N, Teo WS, Yew WS, Chang MW (2017) Engineering a riboswitch-based genetic platform for the self-directed evolution of acid-tolerant phenotypes. *Nat Commun* 8: 411
- Phillips BL, Perkins TA (2019) Spatial sorting as the spatial analogue of natural selection. *Theor Ecol* 12: 155–163
- Piatkevich KD, Jung EE, Straub C, Linghu C, Park D, Suk H-J, Hochbaum DR, Goodwin D, Pneumatikakis E, Pak N et al (2018) A robotic multidimensional directed evolution approach applied to fluorescent voltage reporters. *Nat Chem Biol* 14: 352–360
- Ping D, Wang T, Fraebel DT, Maslov S, Sneppen K, Kuehn S (2020) Hitchhiking, collapse, and contingency in phage infections of migrating bacterial populations. *ISME J* 14: 2007–2018
- Ploss M, Kuhn A (2010) Kinetics of filamentous phage assembly. *Phys Biol* 7: 045002
- Rakonjac J, Model P (1998) Roles of pIII in filamentous phage assembly. *J Mol Biol* 282: 25–41
- Ramirez KS, Snoek LB, Koorem K, Geisen S, Bloem LJ, Ten Hooven F, Kostenko O, Krigas N, Manrubia M, Cakovic D et al (2019) Range-expansion effects on the belowground plant microbiome. *Nat Ecol Evol* 3: 604–611
- Raskin CA, Diaz GA, McAllister WT (1993) T7 RNA polymerase mutants with altered promoter specificities. *Proc Natl Acad Sci USA* 90: 3147–3151
- Ravikumar A, Arzumanyan GA, Obadi MKA, Javanpour AA, Liu CC (2018) Scalable, continuous evolution of genes at mutation rates above genomic error thresholds. *Cell* 175: 1946–1957
- Richter MF, Zhao KT, Eton E, Lapinaite A, Newby GA, Thuronyi BW, Wilson C, Koblan LW, Zeng J, Bauer DE et al (2020) Phage-assisted evolution of an adenine base editor with improved Cas domain compatibility and activity. *Nat Biotechnol* 38: 883–891
- Rong M, He B, McAllister WT, Durbin RK (1998) Promoter specificity determinants of T7 RNA polymerase. *Proc Natl Acad Sci USA* 95: 515–519
- Shih HY, Mickalide H, Fraebel DT, Goldenfeld N, Kuehn S (2018) Biophysical constraints determine the selection of phenotypic fluctuations during directed evolution. *Phys Biol* 15: 065003
- Shine R, Brown GP, Phillips BL (2011) An evolutionary process that assembles phenotypes through space rather than through time. *Proc Natl Acad Sci USA* 108: 5708–5711

- Smeal SW, Schmitt MA, Pereira RR, Prasad A, Fisk JD (2017a) Simulation of the M13 life cycle I: assembly of a genetically-structured deterministic chemical kinetic simulation. *Virology* 500: 259–274
- Smeal SW, Schmitt MA, Pereira RR, Prasad A, Fisk JD (2017b) Simulation of the M13 life cycle II: investigation of the control mechanisms of M13 infection and establishment of the carrier state. *Virology* 500: 275–284
- Tabor JJ (2012) Modular gene-circuit design takes two steps forward. *Nat Methods* 9: 1061–1063
- Thuronyi BW, Koblan LW, Levy JM, Yeh WH, Zheng C, Newby GA, Wilson C, Bhaumik M, Shubina-Oleinik O, Holt JR et al (2019) Continuous evolution of base editors with expanded target compatibility and improved activity. *Nat Biotechnol* 37: 1091
- Walther G-R, Post E, Convey P, Menzel A, Parmesan C, Beebee TJC, Fromentin J-M, Hoegh-Guldberg O, Bairlein F (2002) Ecological responses to recent climate change. *Nature* 416: 389–395
- Wang T, Badran AH, Huang TP, Liu DR (2018) Continuous directed evolution of proteins with improved soluble expression. *Nat Chem Biol* 14: 972–980
- Wong BC, Mancuso CP, Kiriakov S, Bashor CJ, Khalil AS (2018) Precise, automated control of conditions for high-throughput growth of yeast and bacteria with eVOLVER. *Nat Biotechnol* 36: 614–623
- Wu H, Wei T, Yu B, Cheng R, Huang F, Lu X, Yan Y, Wang X, Liu C, Zhu B (2021) A single mutation attenuates both the transcription termination and RNA-dependent RNA polymerase activity of T7 RNA polymerase. *RNA Biol* 18: 451–466



**License:** This is an open access article under the terms of the [Creative Commons Attribution](https://creativecommons.org/licenses/by/4.0/) License, which permits use, distribution and reproduction in any medium, provided the original work is properly cited.